Oscillatory ductile compaction dynamics in a cylinder

Lina Uri,* Dag Kristian Dysthe, and Jens Feder
Physics of Geological Processes, University of Oslo, P.O. Box 1048 Blindern, N-0316 Oslo, Norway
(Received 20 October 2005; revised manuscript received 3 May 2006; published 11 September 2006)

Ductile compaction is common in many natural systems, but the temporal evolution of such systems is rarely studied. We observe surprising oscillations in the weight measured at the bottom of a self-compacting ensemble of ductile grains. The oscillations develop during the first ten hours of the experiment, and usually persist through the length of an experiment (one week). The weight oscillations are connected to the grain-wall contacts, and are directly correlated with the observed strain evolution and the dynamics of grain-wall contacts during the compaction. Here, we present the experimental results and characteristic time constants of the system, and discuss possible reasons for the measured weight oscillations.

DOI: 10.1103/PhysRevE.74.031301 PACS number(s): 81.05.Rm, 83.80.Fg, 83.50.Rp

I. INTRODUCTION

The stress distribution in dry granular media have been studied for more than a century. The German engineer Janssen studied the apparent weight at the bottom of a silo as function of its filling height [1]. Janssen found that the pressure at the bottom of a container of granular material increases linearly with small filling heights, but approaches a constant level exponentially slowly for large filling heights. That the measured weight at the bottom is less than the total weight of grains is referred to as a screening effect. It is well known that the screening effect is due to the grain-wall friction and how the stress distributes in a granular ensemble [2]. Janssen's mathematical expression for this, the Janssen law, compares surprisingly well to experiments [3,4], in spite of its crude assumptions regarding friction and stress distribution [5]. Over the last decade, various aspects of the stress distribution in static granular media have been studied. Experiments have shown that the stress distribution is sensitive to the deposition history [6], the shape and size distribution of grains [7], elastic properties of the base [8] and grains [9], and that an exponential size distribution of forces is found at the bottom of a container for forces larger than the average [10,11]. The stress distribution in dynamic systems has been investigated in pushed columns of granular media inside a cylinder [3,12–14] by measuring the normal force at the bottom for constant driving velocities. At small velocities, the measured force has a stick-slip behavior [14,15] that is probably related to aging of the grain-wall friction due to capillary condensation and shear strengthening of the contacts at the walls [14]. These dynamic systems consist of elastic particles, and the time dependence studied relate to other properties than the particle rheology. There is an essential difference between packings of elastic particles that follow the Janssen law and ductile particles. Ductile particles will yield under load, redistribute forces, and over time simply compact to obtain an equilibrium stress distribution. In the case of a viscous material, the hydrostatic pressure distribution of a fluid will result, with the total weight carried by the bottom.

In Nature, and in many technological processes, slowly compacted or sheared systems are dominated by the deformation of particles. Examples are the pressing of metal and plastic powders, and the compaction of sediments on geological time scales. The time dependence in these systems is mainly given by the plastic properties of the grains and their interactions to boundaries.

Here we mainly present the results from experiments on granular media consisting of viscous deforming grains in a cylinder. This system deformed slowly under its own weight, compacting 10 % in a week, while the normal force f at the bottom was found by using a balance to measure the apparent mass $m_a=f/g$, where g is acceleration of gravity. We found the surprising result that the approach to the final hydrostatic equilibrium was extremely slow, and had a rich dynamical behavior with oscillations and microslips. The response was qualitatively different in the systems with high or low wall friction, and at intermediate friction the apparent mass oscillated, resembling the stick-slip seen in driven hard (elastic) granular systems. The granular structure was not necessarily for these oscillations to occur, but the rheology of the material and the frictional interaction with the wall were essential. The experiments and results are described in the following two sections, while some proposed mechanisms for the oscillations are discussed in Sec. IV. We propose that the observed oscillations are due to two competing effects: slow flow due to relaxation under gravitation and opposing grain wall interaction.

II. EXPERIMENTS

We performed 30 experiments in which an ensemble of N deformable grains were left to compact in a Plexiglas cylinder of diameter D. N was varied between 100–660, and D was between 3.0–6.7 cm. The filling height $h(0)$ at $t=0$ was varies between 1–4 times the cylinder diameter. The system was studied in several ways, but mainly by measuring the apparent mass m_a at the bottom of the cylinder in order to follow the overall evolution of the stress distribution in the compacting ensemble. A Mettler PM4800 balance was used to measure the apparent mass. This balance operates by an induction mechanism that keeps the vertical position of the measurement area stable. To test whether the balance posi-

*Electronic address: l.l.uri@fys.uio.no

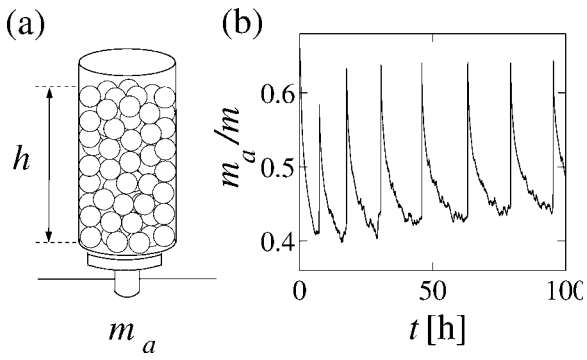

FIG. 1. (a) Schematic illustration of the setup. Ductile grains were filled to a height h in a cylinder and left to compact while the apparent mass m_a at the bottom was measured. (b) A typical recording of the apparent mass (shown normalized by the total mass m of the grains) as a function of time.

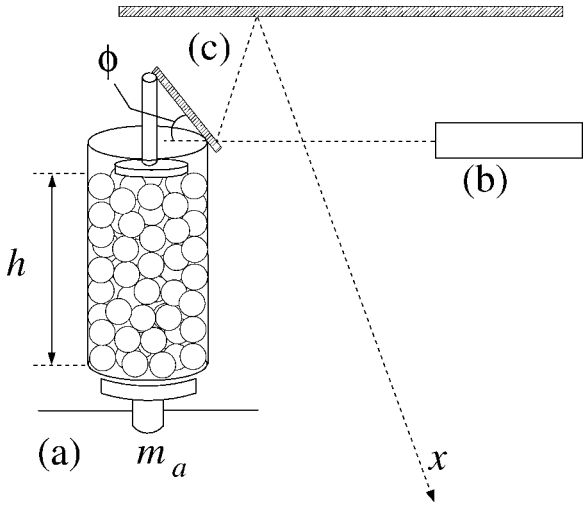

FIG. 2. Illustration of the experimental setup for strain measurement by the use of mirrors and laser. A balance (a) recorded the apparent mass m_a at the bottom of the cylinder. The height of the packing was measured as a function of time by a laser (b) beam that was reflected in a small and a large mirror (c), onto a point on the floor x. The position x moved to the left as the angle ϕ between the small mirror and the horizontal plane was reduced, following the reduction of the height h of the compacting grains. The piston rested on grains that did not touch the walls, thus the strain was measured along a central axis.

tion affected the weight reading the vertical position was recorded using a LVDT displacement sensor (RS, LD400-5) during one experiment. Using a 16 bit DAQ-card (NI, PCI-6034E) 1000 measurements were obtained per second and averaged, resulting in a noise level of ± 0.2 μm. Over 25 hours (four oscillations in weight) the LVDT reading was within ± 0.5 μm, thus the balance did not influence the stress evolution of the packing. The weight was measured to a precision of 0.03 g, and was typically a fraction $(2-3)\times 10^{-4}$ of the total mass of the grains. The cylindrical container was mounted outside of the measurement area. Spherical grains were prepared manually from Play-Doh (Hasbro International Inc., UK) to a diameter $d=(8.8\pm 0.2)$ mm, and poured into the cylinder approximately ten at a time. The initial packing fractions were in the range $c=0.5-0.6$. The material made mainly from salt, water, and flour, and its rheology was measured with a Paar-Physica MCR 300 rheometer to be viscous over a large range of strain rates, $\dot{\varepsilon}=(10^{-2}-10^{-6})$ s^{-1}, with a viscosity of $\mu=3\times 10^5$ Pa s. A schematic illustration of the setup is shown in Fig. 1(a) along with the typical result of the observed weight as a function of time. The measured apparent mass m_a presented in Fig. 1(b) has been normalized by the total mass m of the grains in the cylinder. The apparent mass was found to oscillate in a quasiperiodic manner. The period depended on details of the packing, and could increase or decrease slightly over the duration of each experiment.

In two experiments the total height $h(t)$ of compacting (granular) ensembles were measured using two different setups. A camera was used in one experiment to take pictures of the compaction process at various times. Image analysis was then used to extract the height of the ensemble based on the position of the uppermost 6 grains, to a resolution of 46 μm. In another experiment, the height in the middle of the granular column was recorded by the use of a laser and two mirrors. A small, lightweight piston was placed on top of the central grains and allowed to move only vertically. A small mirror was hinged onto the top of the piston, its lower end resting on the upper cylinder rim. As the grains compacted, the mirror was tilted, reducing its angle ϕ to the horizontal plane. A laser beam was reflected in the small mirror, and again in another, larger, mirror so that the beam was visible as a point on the floor. The position of this point was recorded manually with time, and the height of the granular ensemble calculated to a precision of 3 μm. The piston was positioned along the central axis of the container, and followed the motion of the internal grains that did not touch the wall. Figure 2 illustrates the second strain measurement method. From the measurements of the total height the global strain ε was found as $\varepsilon=1-h(t)/h(0)$.

The dynamics of the grain contacts at the cylinder wall was studied using a camera (AstroCam, Capella, LSR Life Science Resources, UK) in one experiment. The camera had a spatial resolution of 2000×3000 square pixels, and 14 bit intensity resolution. The contrast between the intensity inside and outside of a contact area was within an 8 bit subset of the 14 bit dynamic range. The rim of a contact was established within two pixels with the spatial and intensity resolutions as specified. The uncertainty that one extra rim of pixels introduced to the area of a contact could be as high as 20% for the smallest contact areas. The precision of the center-of-mass position was, however, much better, as it does not depend on the exact choice of thresholding for the contact area.

The cylinder containing the ductile ensemble was placed in front of two mirrors which were set in an angle of 72° to each other. The cylinder was reflected twice in each mirror, thus the camera view held five versions of the cylinder (I–V), capturing it from all sides. The grains' contacts to the wall were literally highlighted by shining light down the Plexiglas wall of the cylinder. The light only reflected out of the wall in areas where the difference in refraction indices were smaller than that between Plexiglas and air, thus the contacts

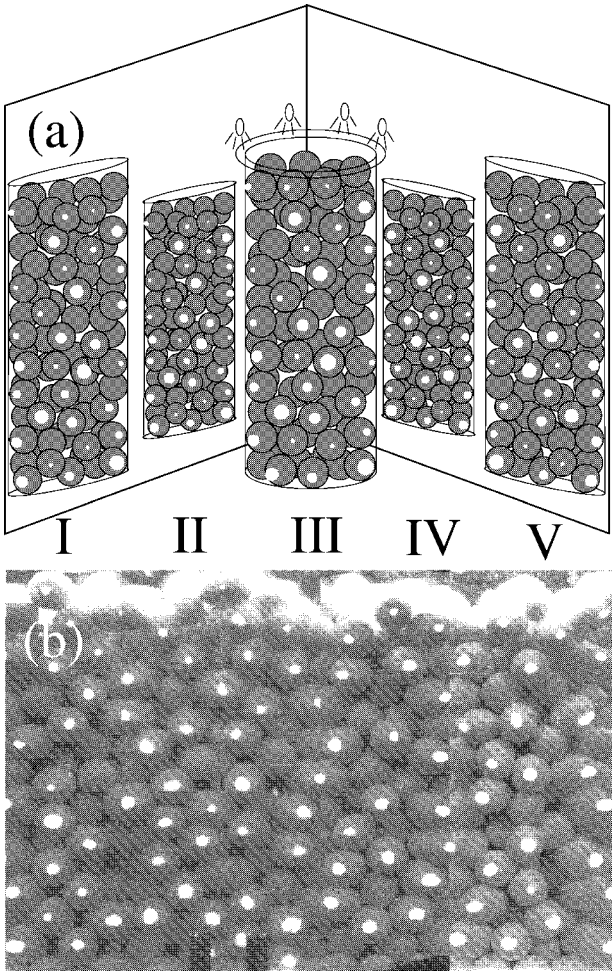

FIG. 3. (a) Schematic drawing of the setup for the measurement of contact areas at the wall of the cylinder. Two mirrors in an angle 72° to each other reflect the cylinder surface and the total area can be extracted. Light emitting diodes were fitted into the top of the cylinder wall to enhance the contrast between contact regions (white) and regions of no contact (gray). (b) The unwrapped [16] surface after image treatment. Each of the five (I–V) cylinder images is scaled and unwrapped before they are fitted in overlapping regions. The match is only at the cylinder surface, which is why the internal regions seem mismatched in some places

between grains and wall were bright in contrast to the pore space. Figure 3(a) illustrates the setup. Each of the five cylinder images I–V (see Fig. 3) was then "unwrapped" [16] and scaled according to the geometry of the setup, then put together to form a continuous image of the surface area of the cylinder. An example of the resultant image is shown in Fig. 3(b). The spatial resolution in these images was 160 μm. Images were recorded every 10 or 20 minutes for two days in order to capture several oscillations. A total of 90 contacts were recovered, and 79 of these were used in the analysis. The remaining 11 contacts were discarded because of some mismatch of their area across boundaries between cylinder images.

An increase of the contact area of 70% was observed during the 60 h that images were recorded, 60% during the first 20 h of compaction, and 10% in the time interval $t \in [20,60]$ h. A contact diameter was defined as $2\sqrt{A/\pi}$ for each contact area A, and found as a function of time. The average contact diameter d_c was found by first taking the average value of each contact diameter over the series of time steps in $t \in [20,60]$, and then find the average of this set, $d_c = 2.66 \pm 0.02$ mm.

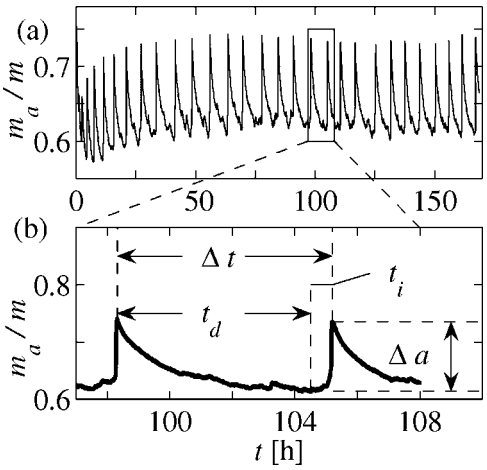

FIG. 4. (a) The evolution of the normalized apparent mass m_a/m as a function of time. (b) Closeup of one period. The total period Δt is the time between two peaks. t_d is the time through which the apparent mass decreases in one period, while t_i is the time of increasing apparent mass. $\Delta a = \Delta m_a/m$ is the amplitude of an oscillation. A subscript n is added to these parameters when they describe the specific values in oscillation number n.

III. RESULTS

A. Characteristics

The typical behavior of the apparent mass m_a in an experiment is as follows. At time $t=0$ all grains have been poured into the cylinder. The apparent mass increases slightly over a period of a few minutes, reaches its maximum (often a global maximum) and then starts to decrease. Weight oscillations mostly initiate during this decrease. When oscillations have developed, their minima decrease toward a global minimum of m_a, before they increase slowly toward a plateau. The plateau varies between experiments in the range 45–88 % of the total mass m of the grains, but are mostly in the range 60–80 %.

Figure 4 illustrates the definition of the periods, intervals, and amplitude of an oscillation, which will be referred to in the following. The period Δt of one oscillation is defined as the time between peaks i and $(i+1)$. This period can be further divided into intervals t_d and t_i of overall decrease and increase, respectively, of the apparent mass. The point of minimum apparent mass between peaks i and $(i+1)$ marks the transition between the regions t_d and t_i, see Fig. 4(b). The amplitude Δa of one oscillation is the change in normalized apparent mass m_a/m during t_i.

The weight oscillations initially have small amplitudes Δa which increase toward a maximum after typically 3–16 oscillations. The amplitudes reduce somewhat after this maximum value; in some experiments they nearly disappear after

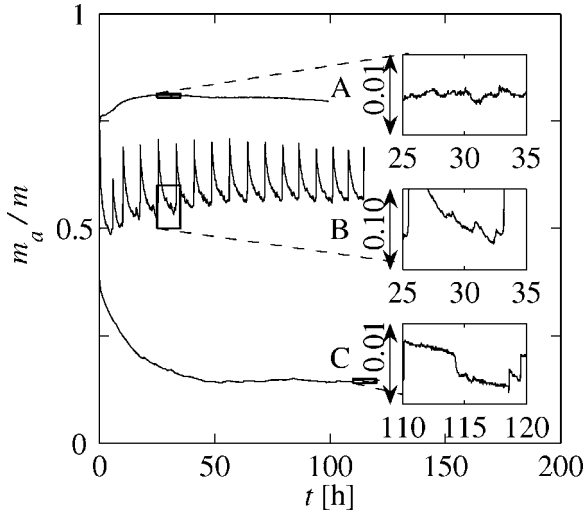

FIG. 5. The resulting apparent masses for different surface treatments: Curve A was the result of coating the walls with Teflon (low friction). No coating of the Plexiglas wall resulted in curve B. Gluing sandpaper to the wall to enhance surface friction gave curve C. The insets to the right show details of each curve (microslips).

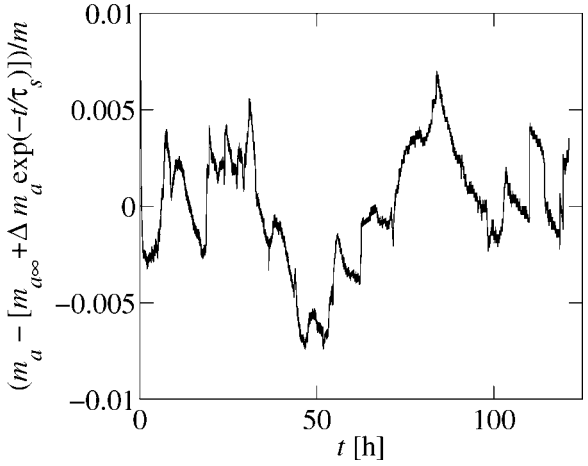

FIG. 6. Deviations of the fit from the measured normalized apparent mass m_a/m as a function of time t for the sandpaper experiment, see Eq. (1).

100 h, while in others they are still at their maximum value after 200 h. The period Δt of an oscillation also tends to increase initially, and then stabilize at a constant value after typically 17–80 h. In a few cases the period only stabilized after 150 h, or not at all in the time span of the particular experiment. During t_d, irregularities larger than the typical noise level occur in m_a/m in most of the experiments, see Fig. 5, curve B. These irregularities are referred to as "microslips" in the following. Technically, a microslip dm_a^+ is defined as the increase of m_a/m in time intervals where the time derivative of m_a is positive.

B. Variations

The observed oscillations in the apparent mass measured under the ductile granular ensemble was seen for all cylinder diameters and filling heights, and proved very robust to most perturbations applied to the system. Varying the cylinder diameter and the filling height of grains did not affect the amplitudes and periods in any consistent manner. Two otherwise equal experiments could produce different characteristics, in one case giving amplitudes of 6% and 20%, and periods of 3.8 and 7.3 h, respectively. The median amplitude and period of 18 processed experiments were $\overline{\Delta a}=5.3[-0.8,3.7]\%$ and $\overline{\Delta t}=3.8[-1.8,2.5]$ h, respectively, where the brackets present quartiles. This rather large variability is probably because details of the packing and the geometry of contacts determine the force distribution so that the compaction is history dependent and not self-averaging. A large variation is also expected due to the small system as we see correlations on length scales of the same order at the system size.

C. Wall friction

Changing the surface properties on the cylinder wall was the only perturbation that dramatically affected the oscillations. Figure 5 shows results from experiments in which the surface friction was reduced by Teflon (curve A), and enhanced by (400 grit) sandpaper (curve C). In the following these experiments are referred to as "the Teflon" and "the sandpaper" experiments, respectively. No alteration was done to the surface of the wall in the experiment that produced curve B, which, apart from the surface, was identical to the Teflon and sandpaper experiments. As can be seen from the figure, reducing or enhancing the wall friction both removed the weight oscillations. By reducing the friction on the wall the apparent mass increased slightly from the initial value (curve A, Fig. 5), and increasing the friction resulted in a decrease of m_a/m (curve C, Fig. 5).

D. Microslips

Fluctuations in the apparent mass are seen in all three curves of the Teflon, the sandpaper, and the regular experiments (see insets of Fig. 5). In order to study the fluctuations the sandpaper curve and the decreasing parts of the oscillations have been fitted with appropriate functions in order to obtain the deviations from the fits. The initial 25 h of the Teflon curve had a complicated functional form that we have been unable to express in a simple form, thus the fluctuations on the Teflon curve were not obtained, but were seen to be of order 1.5×10^{-3}, larger than the noise level of 4×10^{-4}.

The sandpaper curve was well fitted by

$$m_a/m = (m_{a\infty} + \Delta m_a \exp[-t/\tau_s])/m, \tag{1}$$

where $m_{a\infty}=(7.027\pm0.001)$ g, $\Delta m_a=(10.830\pm0.005)$ g, and τ_s is a characteristic time constant of (13.52 ± 0.01) h. The uncertainties are the likely error in the best fit parameters. Figure 6 shows the deviations between the data and the fit $(m_a-m_{a\infty}+\Delta m_a \exp[-t/\tau_s])/m$. The exponential decay fits the observation exceptionally well, and the deviations are within the range $[-0.0077,0.0076]$ of the normalized data. Nevertheless, microslips are easily recognizable above the experimental noise, which is of the order of 2×10^{-4} (0.03 g/142.6 g) of the normalized apparent mass,

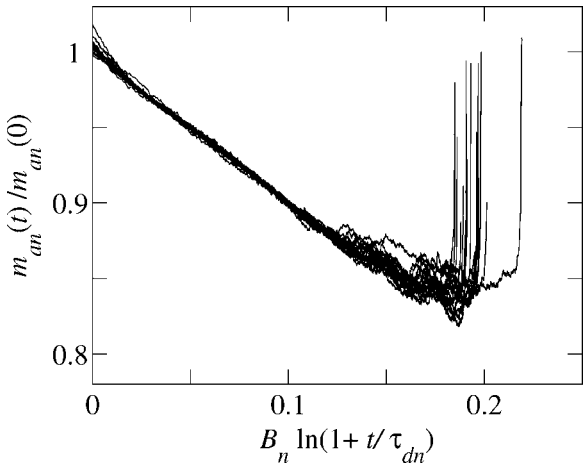

FIG. 7. The decreasing apparent mass of 17 oscillations in one experiment [see Fig. 4(a)] plotted as a function of time according to Eq. (2). [The expression on the horizontal axis is the time-dependent part of Eq. (2).]

while the slips are of the order of 7×10^{-3}, see the lower inset of Fig. 5. The experimental noise is not visible in the figure.

A fit has also been made to the decreasing part t_d of each oscillation n in the curve of Fig. 4(a), which is consistent with logarithmic decay with time:

$$\frac{m_{an}(t)}{m_{an}(0)} = (1 - B_n \ln[1 + t/\tau_{dn}]). \tag{2}$$

Here, $m_{an}(t)$ is the apparent mass of the nth oscillation, and $m_{an}(0)$, B_n, and τ_{dn} are best fit parameters to the equation, calculated for each oscillation n separately. $m_{an}(0)$ is the best fit value of m_{an} at the start of the decrease, based on the first 2.5 h of the decreasing m_{an}. $m_{an}(0)=76.4$ [−0.4, 0.5] g is the median value of $m_{an}(0)$, with the quartile deviations in brackets. $B_n=0.042$ [−0.002, 0.004] is the median of the set of dimensionless constants B_n, and $\tau_{dn}=0.16$ [−0.02, 0.03] h is the median and quartiles of the set of τ_{dn}. Figure 7 shows the collapse of the weight data when plotted according to Eq. (2). The limited dynamic range on both axes suggests that one can also fit the data by a power law with a small exponent. We have not found any theoretical arguments for the choice of one fit over the other, thus the main observation is that the decreasing parts of the oscillations have the same form over the first 2.5 h, with a time constant of $\tau_{dn}=0.16$ h. The sandpaper gave a decreasing exponential function with time, as gives the initial decrease of m_a during t_d in an oscillation:

$$\lim_{t\to 0} 1 - B\ln(1 + t/\tau_d) \simeq 1 - Bt/\tau_d$$

$$\simeq \exp(-Bt/\tau_d) = \exp(-t/\tau_0). \tag{3}$$

The functional dependence is thus similar to the sandpaper at the start of the decrease, with a time constant of $\tau_0=\tau_d/B=3.8$ h.

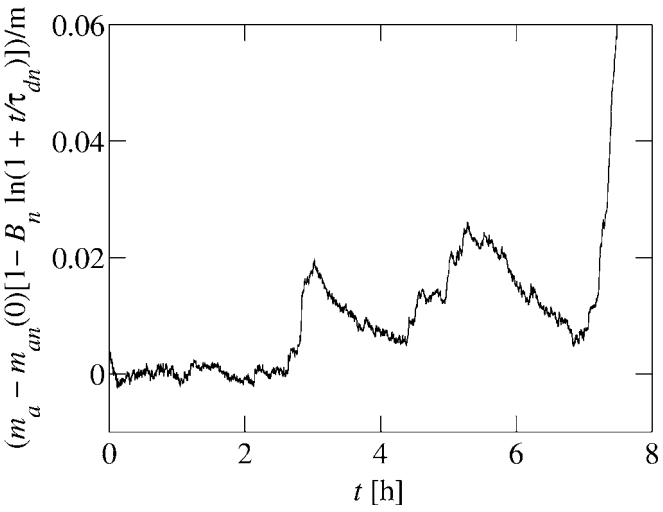

FIG. 8. The deviations from the measured m_a/m of its fit for the decreasing part of one oscillation, as a function of time, see Eq. (2).

The deviation from the fit is plotted for one oscillation in Fig. 8. Large deviations on the order of 2% of the total mass (the microslips) develop some time into t_d (typically 3 h in this experiment). All visible irregularities in this plot is above the noise level of the measurements.

Taking the time derivative of m_a as $dm_a/(mdt)=[m_a(i+1)-m_a(i)]/m[t(i+1)-t(i)]$, the set of positive increments of m_a/m (the microslips, dm_a^+) and negative increments (dm_a^-) were found for each oscillation's t_d. The microslips were removed from the decreasing part of the oscillations by cumulative summation of dm_a^-, and the resulting data set fitted by a power law

$$\sum_n dm_a^-(t) - 1 = -(t/\tau_-)^\alpha. \tag{4}$$

The median and quartiles of the fitting parameters are $\alpha=0.55$ [−0.02, 0.02], and $\tau_-=130$ [−37, 24] h, see Fig. 9. No characteristic time exists for a power law, since $-\lambda^\alpha(t/\lambda\tau)^\alpha$ fits equally well for all λ.

The microslips dm_a^+ were found as a function of time in all the oscillations of the experiment shown in Fig. 4, and

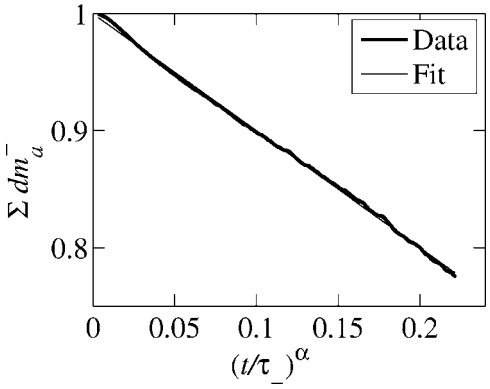

FIG. 9. The cumulative sum of decreasing m_a during an oscillation as a function of the scaled time $(t/\tau_-)^\alpha$, see Eq. (4).

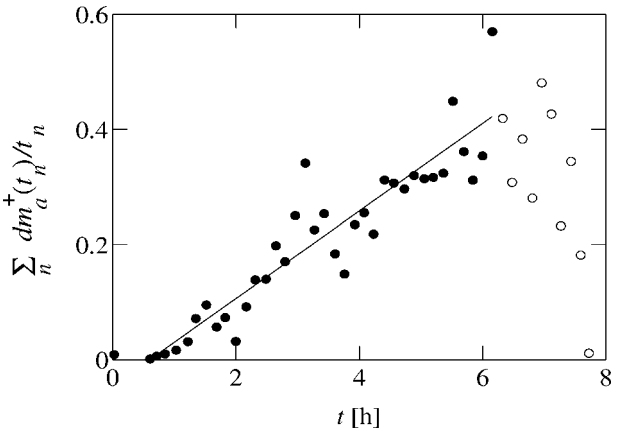

FIG. 10. The microslip "activity" as a function of time after each big slip. The activity is found as the sum of microslips dm_a^+/m from all oscillations in Fig. 4, binned in times t_n and normalized by the width of the bin. See text for symbols.

binned in 50 time intervals. The sum of microslips was taken for each bin, and divided by the size of the bin t_d to produce the temporal evolution of microslip "activity." Figure 10 presents the result. As the t_d were of different lengths for each period, not all bins contain contributions from all oscillations. The bullets present times that include data from all oscillations, whereas a circle includes only data from t_d long enough to contribute to the specific bin. The line through the data is a linear fit, based on all but the first bullet, given by $\Sigma_n m_a^+(t_n)/t_n = A(t-t_0)$. Here, $A=(0.076\pm0.005)$ h^{-2}, and $t_0=(0.6\pm0.2)$ h. The activity presented by the bullet at $t\sim0$ is probably remnants from the big slip that occurred at $t=0$, thus the microslip activity is initiated at time t_0 after each big slip and grows linearly until another big slip occurs.

E. Strains

The measurements of the height of the system as function of time revealed that the vertical motion occurs in steps. This was seen in both strain experiments, and is shown in Figs. 11(a) and 11(c), where the strain has been calculated as $\varepsilon=1-h/h_0$. Figures 11(b) and 11(d) show the simultaneous measurements of the normalized apparent mass $m_a(t)/m$. From the experiment with 3 μm resolution [Fig. 11(a)], the minimum and maximum compaction velocities of the central part of the cylinder were found to be 5.4×10^{-9} m/s and 7×10^{-8} m/s, respectively. The maximum acceleration, occurring at the start of a compaction step, was 1×10^{-11} m/s^2. Comparing the region of decreasing m_a of Fig. 11(b) to the strain in 11(a), a small but visible vertical movement occurs along the central axis of the packing during the weight decrease. The main increase of strain during one oscillation (that is, the step) takes place within the region in which the apparent mass increases from its minimum to its maximum. Unfortunately, the limited resolution of the strain measurements in Fig. 11(c) prevented a detailed comparison between the strain evolution of the six uppermost grains and the apparent mass. It is evident from this measurement, however, that the global strain motion is directly correlated with the

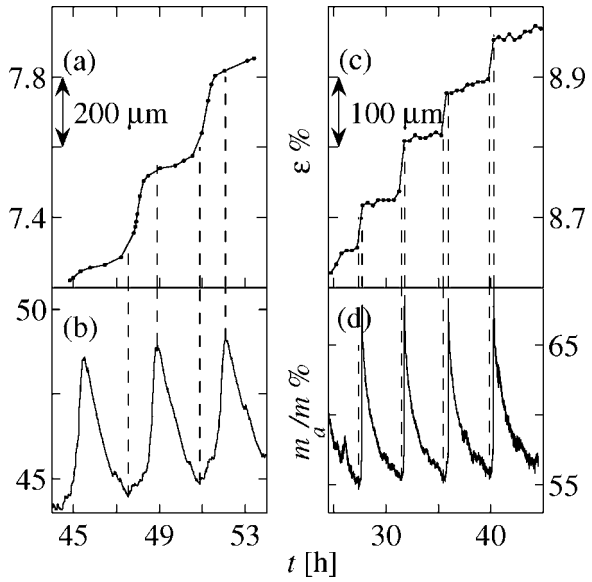

FIG. 11. Details of the strain as a function of time, measured in two experiments compared to the weight m_a. (a) The global strain ε measured with 3 μm resolution (see Fig. 2) as a function of time. (b) The normalized apparent mass m_a/m as a function of time for the experiment in (a). (c) ε measured with 46 μm resolution by the high resolution camera. (d) The apparent mass as a function of time for the experiment in (c).

changes in the apparent mass. A compaction velocity of the uppermost grains of $(0.6-3)\times10^{-9}$ m/s was found during t_d, and 4×10^{-8} m/s during t_i. We note that we have observed steps in the global strain as in Fig. 11(a) also for the case when the cylinder had a fixed bottom.

F. Wall contacts

The dynamics of the wall contacts were studied in one experiment as described in Sec. II. Having found the "unwrapped" properly scaled surface of the cylinder (see Fig. 3), we obtained a high contrast of the contact. The development of the area and center-of-mass position of each contact was followed through the experiment. The weight oscillations correlated strongly to the contacts' center-of-mass motion, while no such correlation was found with the changes in contact area.

The contacts were seen to move "simultaneously," that is, within the temporal resolution of the images, which means they all slipped within a period of 15–20 min, during t_i. Figure 12 shows the cumulative distribution $P(s>\Delta y)$ of vertical contact displacement Δy between two consecutive images. The contact displacement is normalized by the average contact diameter d_c. Each curve corresponds to the distribution in one time step of the experiment. Curves A present the motion during slips, while curves B are the motion in time steps between slips. The gray band through B spans the average ± the standard deviation of vertical motion.

The median vertical displacement of a contact during a slip was 6 $[-1,2]$% of the average contact diameter d_c. Outside of the slips the median displacement was only

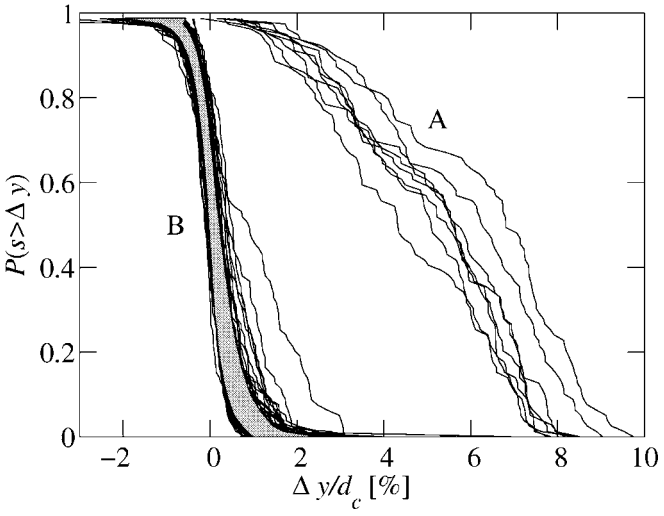

FIG. 12. The cumulative distribution $P(s>\Delta y)$ as a function of normalized vertical contact displacement $\Delta y/d_c$ between two consecutive images. Motion downward has positive values of Δy. Curves A result during slips, while curves B present the remaining movement between time steps. The gray region through B covers the average value taken at each 1/79 interval of P, plus and minus the standard deviation from the average.

0.07 [−0.20,0.24]% of d_c. Figures 13(a)–13(c) show the difference in one contact area between consecutive images in one experiment. White corresponds to new contact area, black to area that was left since the previous image, and light gray shows contact area where no changes occurred. Figures 13(d) shows the normalized apparent mass and the average strain of column at the top and the bottom. The markers in both plots represent the times when pictures were taken. In Fig. 13(d) circles mark the times when 15% of the contacts moved more than 1% of the average contact diameter in 20 min (since the last image). The bullets show the times when 80% of the contacts moved at least 2% of the average contact diameter. Triangles represent the times when pictures were taken. The strain of the compacting column was found based on the average displacement $\langle h(0)\rangle - \langle h(t)\rangle$ of the 20 upper wall contacts (diamonds, A) as $\varepsilon = 1 - \langle h(t)\rangle_A / \langle h(0)\rangle_A$, and similarly for the 20 lower wall contacts (circles, B). From Fig. 13(e) it can be seen that the strain evolves more in the upper region of the packing than in the lower. The compaction is thus not uniform. this might indicate that the lower part of the packing is denser than the upper, and thus compaction occurs slower than in the upper part of the cylinder. The steps in the strain, as observed for the top of the packing in Figs. 11(a) and 11(c), also show up in the contact motion at all heights [Fig. 13(e)]. Based on the observed area of the grain-wall contacts and the measured m_a, the average load per square millimeter carried by a contact was calculated to be in the range (0.5–1.2) kPa.

G. Bulk experiment

One experiment was performed to study the wall contacts separately. The granular ensemble was exchanged with a nonporous slab of Play-Doh that did not fill the cylinder, but

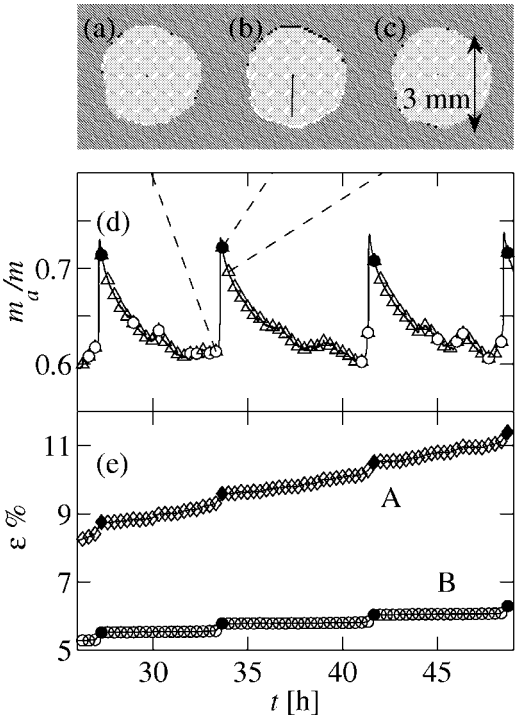

FIG. 13. (a), (b), and (c) show difference images of a contact between consecutive images. White is newly established area, black is area that no longer is a part of the contact, and light gray is the unchanged contact area. The center-of-mass motion between the images are shown as black lines. The length of the lines is exaggerated 10 times. (d) shows the normalized apparent mass, the triangles (△) mark the times when pictures were taken of the ensemble. Circles (○) mark the times when minimum 15% of the contacts moved more than 1% of the average contact diameter. Bullets (●) mark the times when more than 80% of the contacts moved at least 2% of the average contact diameter. The lower plot (e) shows the average strain development found from image analysis for the 20 lower
(○, curve B) and upper (◇, curve A) wall contacts. Filled symbols represent the times that a picture was taken at or immediately after a peak in the apparent mass presented in (d).

rested on the bottom and had 3–4 wall contacts. The geometry of the slab was like a somewhat irregular and bent cylinder of diameter 0.8 times that of the container. This experiment is referred to as "the bulk experiment" in the following. The slab was left to flow into the available space, and the apparent mass was measured as before, see curve B of Fig. 14. Again, a granular version of this experiment was conducted for comparison, in which the total mass of the grains and the cylinder diameter were the same as those of the bulk experiment, see Fig. 14, curve A. As seen from the figure, both setups produced weight oscillations, thus the granular geometry is not the reason for the oscillations. Oscillations started later in the bulk case than in the granular case, and both systems show uncommon irregularities in their periods. The granular system had nearly 100 grain-wall contacts, while the bulk sample had 3–4 large contact areas. The oscillations are probably due to the multicontact nature of the interface between the deforming sample and the confining cylindrical wall.

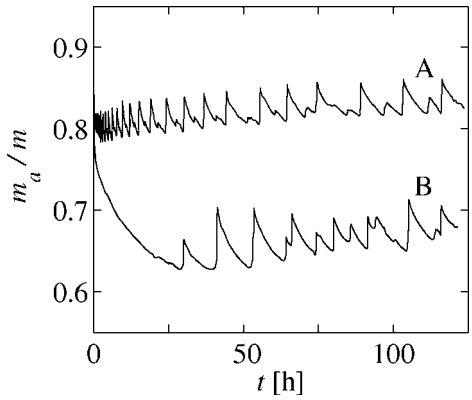

FIG. 14. The normalized apparent mass m_a/m as a function of time t at the bottom of a cylindrical Play-Doh sample (B), as compared to m_a/m from a granular geometry (A) as a function of time.

H. Time and length scales

Table I presents the characteristic values of various parameters. (a) gives the median period, amplitude, intervals t_d and t_i, and characteristic times $\overline{\tau_d}$ and t_0 for the oscillations in one experiment (see Fig. 4). (b) presents the characteristic time from the fit of m_a/m from the sandpaper experiment, and the estimated characteristic time of elastic relaxation (see Sec. IV).

IV. DISCUSSION

The self-compaction of a ductile ensemble depends on the deformability of the grains and on a porous structure. The granular geometry of the ensemble was not necessary for oscillations to form, as weight oscillations also resulted under a bulk slab of material that deformed viscously into available space. This result emphasizes the importance of the wall contact interaction to the observed oscillations in the apparent mass.

TABLE I. (a) Median values of the period $\overline{\Delta t}$, amplitude $\overline{\Delta a}$, the intervals t_d and t_i, the characteristic times $\overline{\tau_d}$ and $\tau_0=\overline{\tau_d}/B$ of decreasing m_a, and t_0 of activation of microslips of the experiment presented in Fig. 4(a). (b) Characteristic times τ_s of the m_a/m evolution in the sandpaper experiment, and τ_e, the estimated time of relaxation of elastic stress. (c) Estimated characteristic length scales, from time scales in (a) and (b), see Sec. IV.

		Characteristic values
(a)	$\overline{\Delta t}$	6.4 [−0.7, 1.2] h
	$\overline{t_d}$	5.2 [−0.3, 1.1] h
	$\overline{t_i}$	0.8 [−0.3, 1.0] h
	$\overline{\tau_d}$	0.16 [−0.02, 0.03] h
	$\tau_0=\overline{\tau_d}/B$	~3.8 h
	t_0	0.6±0.2 h
	$\overline{\Delta a}$	12.6 [−0.3, 1.0]%
(b)	τ_s	13.52±0.01 h
	τ_e	$\sim 10^{-6}$ h
(c)	l_s	~260 μm
	l_0	~74 μm
	l_d	~101 μm
	l_i	~115–200 μm

The grain-wall interaction proved to be crucial to the oscillations in the apparent mass by the experiments with varying wall friction. No oscillations were observed when increasing or decreasing the wall friction from that of the regular experiments with Plexiglas walls. The evolution of m_a in these experiments is interesting because it shows two different behaviors according to the wall friction. A low wall friction resulted in an increasing apparent mass, while a high wall friction made the measured weight decrease. The same mechanisms leading to these results are likely to be the reason for the oscillations observed in m_a in the bulk and regular experiments.

A. m_a decrease and increase

The reason for the decrease of the apparent mass must be that the walls sustain an increasing part of the total grain mass, that is, a dynamic vertical force must act on the grain contacts from the wall. This force could be friction, shear cohesion, or a combination of the two, and will be referred to as the grain-wall interaction in the following.

In principle, elastic energy could be stored in compressed parts of the packing after a slip, resulting in a decreased grain-wall interaction. The relaxation of this elastic energy could cause the observed decrease in the apparent mass. The characteristic time of elastic relaxation is expressed as the ratio of viscosity μ to bulk modulus K. We know that the viscosity of Play-Doh is of the order of 10^5 Pa s for shear rates as low as 10^{-6} s^{-1}. The bulk modulus was not measured, but it is expected to be closer to that typical of fluids ($K_f \simeq 1-2$ GPa [18]) than that of iron ($K_i \simeq 170$ GPa [19]), thus on the order of 10^9 Pa. The resulting estimate of elastic relaxation time for Play-Doh is

$$\tau_e = \mu/K = 10^5/10^9 = 10^{-4}\ \text{s}. \tag{5}$$

Elastic compressive stresses should relax in (less than) seconds, which is much less than any time scale observed in an oscillation.

Another explanation for the decreasing m_a emerges from the assumption that the ratio of horizontal to vertical stresses increases with increasing packing fraction. If friction is assumed to be proportional to the normal force, an increasing horizontal stress in the packing would result in increased wall friction, hence a decrease in m_a. The packing fraction increases approximately 10% during the experiment, while the characteristics of the oscillations does not change. This implies that the packing fraction is not the main parameter for describing the dynamic behavior.

The reason for a decreasing apparent mass can be seen in connection to the shearing of grain-wall contact regions. During the time t_d of decreasing m_a the strain increases very slowly, suggesting that only an internal flow of grains contributes to the strain in this regime [see Figs. 11(a) and 11(b)]. The analysis of the motion of grain-wall contacts shows that the vertical motion of contacts in this regime is

limited and noisy, thus most contacts are practically at rest (even though the central part of the packing creeps). Due to the slow flow internally in the packing, they are also continuously sheared. The wall contacts must also have been sheared in the bulk experiment, as the bent slab slowly deformed and flowed into available space.

B. Microslips

There are clear slips of the order of 2% in the normalized apparent mass during the decreasing part of the period in the granular setups (see Figs. 4 and 8). Microslips are not seen once oscillations have developed in the weight data from the bulk experiment, thus their origin seems to be the granular geometry, or possibly the large difference in the number of wall contacts between the bulk and granular systems. No collective motion is seen at the wall during the microslips in the granular experiment, although 5% of the contacts move a distance of 1% of d_c in every time step, thus their motion might be connected to the measured microslips in m_a. Microslips might be due to the internal reorganization of forces within the system, which may trigger some of the grain-wall contacts into motion. A reorganization of forces must also take place in the material in the bulk experiment, although probably in a different way than that of the more complex granular geometry. The reorganization must increase the average shear stress in the contact regions, which again leads to an increase of the vertical grain-wall interaction. Once a contact experiences a shear stress that cannot be sustained by the grain-wall interaction, it is triggered into motion.

The strain development could not be measured in the sandpaper experiment, thus whether this system compacted much is not known. Similar, but smaller, microslips than those seen in regular experiments were seen in the sandpaper experiment. This suggests that internal stress rearrangement was taking place. The grain-wall interaction was considerably higher in the sandpaper experiment than in the regular setup (as the apparent mass reached a minimum of 15% of the total mass). It is reasonable to assume that the contacts did not move much, or in any correlated manner, based on the lack of weight oscillations.

The direct correspondence between the step in the strain and the increasing m_a in Figs. 11(a) and 11(b) implies that the motion of wall contacts is very important for the weight increase. Assuming that wall contacts are broken, or mobilized, at a critical shear stress, one or more contacts will initiate a slip, and the others follow. The contacts that break contribute to a decrease in the total wall interaction, thus a possible increase of the apparent mass. The sum of wall interactions decreases over a time period that must depend on how fast the contact breaking propagates among the other contacts, and how fast each contact breaks. From our temporal resolution in the study of grain-wall contacts, we see that all grains move within 20 min in connection with the slip. The apparent mass will increase according to the decreasing wall interaction F_w, as the force balance of the system is $\Sigma F = m_a g - F_w = ma < 10^{-12}$ N $\simeq 0$, thus inertial effects are negligible.

The strain development was not measured in the Teflon experiment, thus it is not known whether the strain had similar steps during the compaction as in the regular experiments. Based on the direct correlation between weight oscillations and the observed strain in the regular experiments, however, it seems likely that the wall contacts in the Teflon experiment in some sense moved continuously, as no oscillations in m_a were observed here. Microslips were observed in m_a, however, thus some dynamic interaction between the grains and the wall was present, see the upper inset of Fig. 5. Sliding contacts also support some of the grain mass, as neither during t_i in the regular experiments nor in the Teflon experiment does the apparent mass reach 100 % of the grain mass. The grain-wall interactions during motion are smaller, however, than in the static case, as the apparent mass increases during motion in the regular experiments, see Fig. 11.

That all contacts are mobilized within a time interval corresponding to a slip could imply that, when sufficiently sheared, they are sensitive to changes in the stress distribution, and thus easily triggered. From Fig. 13(d) we see that more than 80% of the contacts move more than 2% of d_c during a slip event, and that 15% move at least 1% of d_c immediately before these slips. In some cases, although not consistently, 15% of the contacts move at least 1% of d_c in connection to microslips. Also, the activity of microslips increases during t_d, which suggests that the system becomes more critical.

C. Time and length

The time scales of the system spans a factor 100, see Table I, ranging from 0.16 to 13.52 h. It is tempting to speculate that these time scales reflect the spatial dimensions in the system, from 1 mm (diameter of small contact area) to 10 cm (filling height). A direct estimate of the maximum length scale can be made from the velocities and the observed time scales. Assuming that the grain-wall contacts in the sandpaper experiment do not slip, the internal flow of velocity $v_d = 5.4 \times 10^{-9}$ m/s with the characteristic time τ_s gives a length scale $l_s = 260$ μm. The corresponding length from the initial exponential decrease of m_a in an oscillation is $l_0 = \tau_0 \times v_d$ m/s $= 74$ μm, and from the t_d and t_i, we get $l_d = t_d \times v_d = 101$ μm and $l_i = t_i \times v_i = 115 - 200$ μm, respectively. v_i is the velocity of the bulk during a slip. The range of l_i results from the different compaction velocities found during t_i in the two experiments presented in Fig. 11. The length scales extracted from the characteristic times span a smaller range than the time scales do, and are much smaller than the macroscopic lengths mentioned above. The small length scales suggest that details of the contact motion might be of importance to the time scales observed in the system.

Flow of viscous fluid along a wall can be described by a Navier length [20]. An average contact velocity v_c during a slip can be found from knowing that contacts slip 6% of the average contact diameter in 20 min, $v_c = 1.15 \times 10^{-7}$ m/s. The amount of fluid slip along a wall is given by the Navier length $b = \mu / k$, where μ is the fluid viscosity and k is the surface friction coefficient given by σ / v_c. The average shear, σ, of a contact was found to be between 0.5–1.2 kPa, thus k is within the range $(2.7 - 11) \times 10^9$ Pa s/m. The Navier

length is then $b \in [27-90]$ μm, slightly smaller, but of the same order as some of the lengths estimated above.

The motion of a contact was not studied with sufficient temporal or spatial resolution to conclude whether the whole contact slid a fraction of d_c at constant velocity, or it slid by self-healing slip pulses [21,22]. Both processes are known from experiments on frictional motion in low velocity sheared systems of (hard) granular systems [15] and slipping of a gel/glass interface [22].

V. CONCLUSIONS

We observe semiregular oscillations in the measured apparent mass m_a at the bottom of a self-compacting ductile grain packing. The oscillations in one particular experiment are on the order of 10% of the total mass m of the grains, and have periods of roughly 6 h. The oscillations persist when the granular setup is exchanged with a bulk sample of the same ductile material, but disappear when the grain-wall interaction is reduced or increased. Grain-wall contacts are seen to move collectively in correspondence to the slip events in m_a, as at least 80% of the contacts move a distance larger than 2% of the average contact diameter during a slip, see Figs. 12 and 13.

The decrease of the apparent mass in an oscillation is thought to be the result of shearing of static wall contacts between grains and the container wall. The slow ductile flow internally in the cylinder causes a dynamic stress distribution, which results in a continuous increase of the shear stress at the grain-wall contacts. This continuous increase is the reason for the decreasing apparent mass.

"Microslips" of the order of 2% are seen in the normalized apparent mass m_a/m during the decrease, which probably result from internal stress redistribution in granular setups, as they were not seen in m_a of the bulk experiment. The microslips correspond in some cases to limited grain-wall contact motion, and their "activity" increases during the interval of decreasing m_a. These slips are also seen when the grain-wall interaction is reduced or enhanced, that is, when contact motion is stimulated or repressed.

Different characteristic times have been found from curve fitting of the apparent mass evolution during the "sandpaper" experiment and the decreasing part of oscillations in one experiment. We have also estimated a typical time scale of relaxation of elastic compressive stresses, and concluded that elasticity is not the driving mechanism for the observed oscillations. The characteristic times, together with the period and intervals of increasing and decreasing m_a, are presented in Table I. A successful model should reproduce these characteristic times.

Some attempts at constructing a minimum model have been pursued, but the models were discarded as they depended on a finite acceleration or on unknown microscopic parameters of the system. Further work is necessary to understand the dynamic behavior of the system, and ideas and modeling approaches are welcome.

ACKNOWLEDGMENTS

We wish to thank the Norwegian Research Council for financial support through Grant No. 146031. Many thanks also to Thomas Walmann for help with image analysis, and Renaud Toussaint, Jean Christophe Geminard, Espen Jettestuen, and Yuri Podladchikov for helpful discussions. Thanks to Bo Nyström and Anna-Lena Kjøniksen for viscosity measurements.

[1] H. A. Janssen, Z. Vereines Deutscher Ingenieure **39**, 1045 (1895).
[2] J. Duran, *Sands, Powders, and Grains* (Springer-Verlag, New York, 1999).
[3] D. Arroyo-Cetto, G. Pulos, R. Zenit, M. A. Jiménez-Zapata, and C. R. Wassgren, Phys. Rev. E **68**, 051301 (2003).
[4] L. Vanel, P. Claudin, J. P. Bouchaud, M. E. Cates, E. Clément, and J. P. Wittmer, Phys. Rev. Lett. **84**, 1439 (2000).
[5] P. G. de Gennes, Rev. Mod. Phys. **71**, S374 (1999).
[6] L. Vanel, D. Howell, D. Clark, R. P. Behringer, and E. Clément, Phys. Rev. E **60**, R5040 (1999).
[7] J. Geng, D. Howell, E. Longhi, R. P. Behringer, G. Reydellet, L. Vanel, E. Clément, and S. Luding, Phys. Rev. Lett. **87**, 035506 (2001).
[8] R. Brockbank, J. M. Huntley, and R. C. Ball, J. Phys. II **7**, 1521 (1997).
[9] J. M. Erikson, N. W. Mueggenburg, H. M. Jaeger, and S. R. Nagel, Phys. Rev. E **66**, 040301 (2002).
[10] C. H. Liu, S. R. Nagel, D. A. Schecter, S. N. Coppersmith, S. Majumdar, O. Narayan, and T. A. Witten, Science **269**, 513 (1995).
[11] G. Lovoll, K. J. Maloy, and E. G. Flekkoy, Phys. Rev. E **60**, 5872 (1999).
[12] Y. Bertho, F. Giorgiutti-Dauphiné, and J.-P. Hulin, Phys. Rev. Lett. **90**, 144301 (2003).
[13] G. Ovarlez, C. Fond, and E. Clément, Phys. Rev. E **67**, 060302(R) (2003).
[14] G. Ovarlez and E. Clément, Phys. Rev. E **68**, 031302 (2003).
[15] S. Nasuno, A. Kudrolli, A. Bak, and J. P. Gollub, Phys. Rev. E **58**, 2161 (1998).
[16] The imaged projection of the curved surface was scaled to that of a flat plane, reproducing the surface as seen normal to the curved container wall.
[17] L. Uri, T. Walmann, L. Alberts, D. K. Dysthe, and J. Feder, Phys. Rev. E **73**, 051301 (2006).
[18] *Science Data Book*, edited by R. M. Tennent (Oliver and Boyd, Twenty-first impression, Edinburgh, 1971).
[19] F. Cardarelli, *Materials Handbook. A Concise Desktop Reference* (Springer-Verlag, London, 2000).
[20] P. G. de Gennes, Langmuir **18**, 3413 (2002).
[21] E. Gerde and M. Marder, Nature (London) **413**, 285 (2001).
[22] T. Baumberger, C. Caroli, and O. Ronsin, Phys. Rev. Lett. **88**, 075509 (2002).